

Layer-by-Layer Organic Solar Cells Enabled by 1,3,4-Selenadiazole-  
Containing Crystalline Small Molecule with Double-Fibril Network  
Morphology

X. Chen, R. Li

To be published in "Angewandte Chemie International Edition"

May 2024

Photon Sciences

**Brookhaven National Laboratory**

**U.S. Department of Energy**

USDOE Office of Science (SC), Basic Energy Sciences (BES)

Notice: This manuscript has been authored by employees of Brookhaven Science Associates, LLC under Contract No.DE-SC0012704 with the U.S. Department of Energy. The publisher by accepting the manuscript for publication acknowledges that the United States Government retains a non-exclusive, paid-up, irrevocable, world-wide license to publish or reproduce the published form of this manuscript, or allow others to do so, for United States Government purposes.

## **DISCLAIMER**

This report was prepared as an account of work sponsored by an agency of the United States Government. Neither the United States Government nor any agency thereof, nor any of their employees, nor any of their contractors, subcontractors, or their employees, makes any warranty, express or implied, or assumes any legal liability or responsibility for the accuracy, completeness, or any third party's use or the results of such use of any information, apparatus, product, or process disclosed, or represents that its use would not infringe privately owned rights. Reference herein to any specific commercial product, process, or service by trade name, trademark, manufacturer, or otherwise, does not necessarily constitute or imply its endorsement, recommendation, or favoring by the United States Government or any agency thereof or its contractors or subcontractors. The views and opinions of authors expressed herein do not necessarily state or reflect those of the United States Government or any agency thereof.

# Layer-by-Layer Organic Solar Cells Enabled by 1,2,4-Selenadiazole-Containing Crystalline Small Molecule with Double-Fibril Network Morphology

*Xuyang Chen, Yinfeng Li, Wenwen Jing, Tao Zhou, Xiaopeng Xu,\* Yuwei Duan, Liyang Yu, Ruipeng Li, and Qiang Peng\**

X. Chen, Y. Li, W. Jing, T. Zhou, Dr. X. P. Xu, Dr. L. Y. Yu, Prof. Q. Peng

School of Chemical Engineering and State Key Laboratory of Polymer Materials Engineering, Sichuan University, Chengdu 610065, P. R. China.

Email: xpxu@scu.edu.cn; qiangpeng@scu.edu.cn

Dr. Y. Duan, Prof. Q. Peng

College of Materials and Chemistry & Chemical Engineering, Chengdu University of Technology, Chengdu 610059, P. R. China.

Dr. R. P. Li

National Synchrotron Light Source II Brookhaven National Lab, Suffolk, Upton, NY 11973, USA

Keywords: organic solar cells, layer-by-layer processing, morphology control, nano fibril, small molecule additive

A double-fibril network of the photoactive layer morphology is recognized as an ideal structure facilitating exciton diffusion and charge carrier transport for high-performance organic solar cells (OSCs). However, in the layer-by-layer processed OSCs (LbL-OSCs), polymer donors and small molecule acceptors (SMAs) are separately deposited, and it is challenging to realize a fibril network of pure SMAs with the absence of tight interchain entanglement as polymers. In this work, crystalline small molecule donors (SMDs), named TDZ-3TR and SeDZ-3TR, were designed and introduced into the L8-BO acceptor solution, forcing the phase separation and molecular fibrilization. SeDZ-3TR showed higher crystallinity and lower miscibility with L8-BO acceptor than TDZ-3TR, enabling more driving force to favor the phase separation and better molecular fibrilization of L8-BO. On the other hand, two donor polymers of PM6

and D18 with different fibril widths and lengths were put together to optimize the fibril network of the donor layer. The simultaneous optimization of the acceptor and donor layers resulted in a more ideal double-fibril network of the photoactive layer and an impressive power conversion efficiency (PCE) of 19.38% in LbL-OSCs.

## Introduction

Organic solar cells (OSCs) are promising next generation renewable low-carbon energy technology candidates supporting versatile application scenarios, such as portable, wearable, and internet-of-things (IoT) integrated devices.<sup>[1-4]</sup> In the last few years, great efforts devoted to new materials design and delicate devices engineering have successfully pushed the power conversion efficiency (PCE) up to over 19% benchmark.<sup>[5-15]</sup> Despite great achievement, the state-of-the-art OSCs predominately employ a bulk heterojunction (BHJ) photoactive layer in the devices, which is rather complicated and far from being well controlled and fully understood. To be specific, the BHJ layer is formed by the spontaneous phase separation of a pre-mixed solution of electron donor and acceptor materials, where a bicontinuous and interpenetrating network is recognized to be essential for favoring charge generation and transportation. Nevertheless, such a BHJ structure prepared by the one-step deposition method is highly sensitive to material properties and processing conditions, which often produce the intimately mixed donor and acceptor with non-ideal crystallinity and domain purity.<sup>[16-18]</sup> In addition, the kinetically quenched BHJ morphology is typically in a metastable intermediate state and will further move toward a thermodynamic equilibrium state, resulting in demixing of the mixed phases.<sup>[19-21]</sup> This leads unavoidably to the morphological degradation that is sped up by the low miscibility of donor and acceptor materials or the accumulated heat, bringing long-term stability issues.<sup>[21-22]</sup>

Alternative to the one-step photoactive layer deposition in BHJ-OSCs, layer-by-layer (LbL) processing have recently emerged as a competitive option.<sup>[17-18, 23-36]</sup> As the donor and acceptor are processed sequentially in two steps, the microstructure of each layer can be optimized independently in the LbL-OSCs, without the need to concern about incompatibility issues arising from the thermodynamic

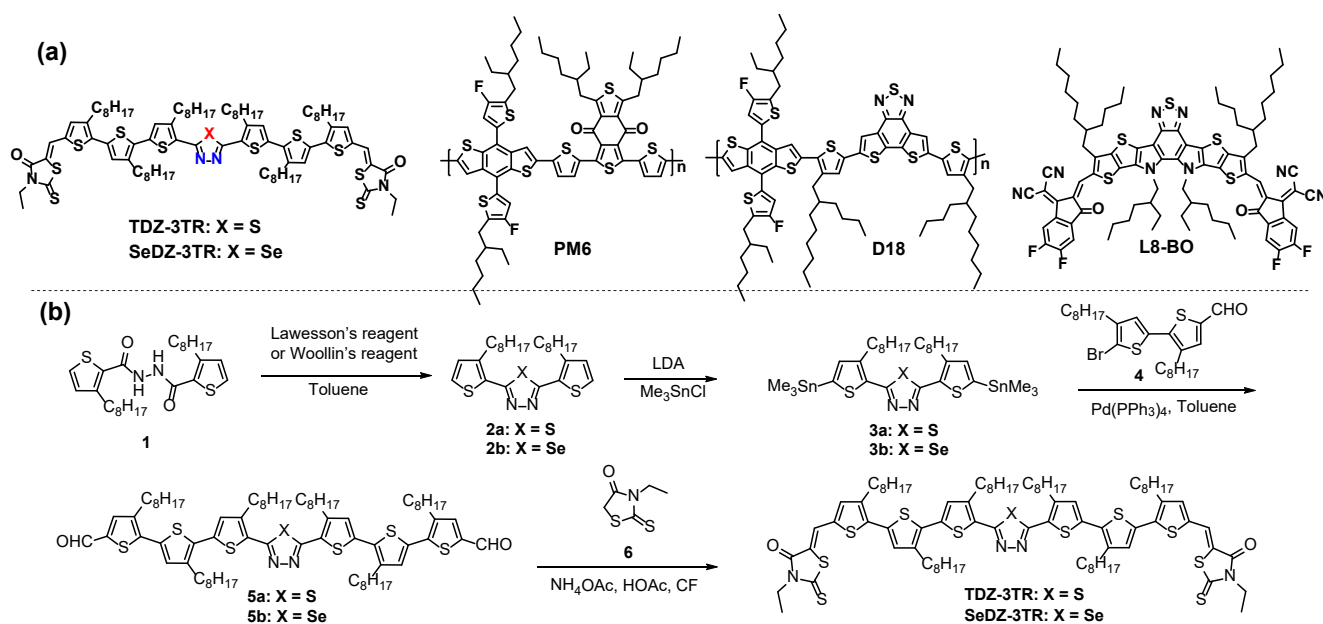
miscibility between different components in the BHJ-OSCs.<sup>[17, 24-26]</sup> Therefore, LbL-OSCs have great potential to avoid the complicated photoactive layer phase separation associated with the BHJ-OSCs, widening the room for fine-tuning the photoactive layer morphology.<sup>[16, 24, 28]</sup> More importantly, the sequentially deposition of donor and acceptor materials also enables the formation of a more favorable vertical component distribution featured with a p-i-n like structure, which not only provides sufficient D/A interfaces but also enables higher purity of donor and acceptor domains, benefiting the exciton dissociation, charge transportation and collection by the respective electrodes.<sup>[25, 31, 37-38]</sup> For these reasons, further breakthroughs in the device performances are expected by rational material design and device engineering for LbL-OSCs.

In developing efficient LbL-OSCs, great efforts have been devoted to modulating the vertical component distribution of donor and acceptor materials, because only the adequately intermixing between these components can provide sufficient D/A interfaces for efficient charge generation and transportation.<sup>[23, 27-33]</sup> As the microstructure of the underlying polymer donor layer plays a decisive role in determining the magnitude of intermixing, thus has attracted extensive studies in recent years.<sup>[18, 29-32, 35-36]</sup> For instance, Sun *et al.* found that the self-assembly of a conjugated polymer donor into a well-defined fibril structure could allow acceptor molecules diffused into the well-developed fibril mesh to form a bicontinuous network morphology in the LbL-OSCs.<sup>[39]</sup> We recently developed a series of polymer additives to assist the self-assembly of the host polymer donor, which finely tuned the nanofibril matrix and optimized the vertical phase separation.<sup>[16]</sup> In contrast, it is challenging to realize a fibril like morphology of small molecular acceptors (SMAs) with the absence of tight interchain entanglement as polymers. The main function of the commonly used additives, such as 1,8-diiodooctane (DIO),<sup>[20, 29, 38, 40-41]</sup> 1-chloronaphthalene (CN),<sup>[31, 42-46]</sup> introduced into the SMA solution have positive effect on improving the crystallinity of the acceptor and swelling the polymer matrix for better vertical segregation.<sup>[29]</sup> However, they could difficultly establish a fibril like structure of the SMA domain in the LbL-OSCs, despite a bicontinuous double-fibril network for both donor and acceptor materials has been demonstrated to be facilitating exciton diffusion and charge carrier transport for high devices performances in the BHJ-

OSCs.<sup>[14]</sup> Most recently, Wang *et al.* introduced a trace amount of polymer donor to help the fibrillization of SMA and successfully realized the bicontinuous fibril networks of the photoactive layer and high performances in the LbL-OSCs.<sup>[47-48]</sup> The results highlighted the importance of properly introducing a donor material into the SMA layer for fibrillization of the latter and obtaining double-fibril network in LbL-OSCs. However, there is still lack of extensive research on the fibrillization of SMAs in LbL-OSCs, and in-depth understanding the effect of SMA fibrillization on the device performance remains elusive.

In this work, we report the simultaneously fibril network optimization of acceptor and donor layers to construct an ideal double-fibril network morphology of the photoactive layer for high performance LbL-OSCs. To assist the fibrillization of (2,2'-((2Z,2'Z)-((12,13-bis(2-ethylhexyl)-3,9-bis(2-butyloctyl)12,13-dihydro-[1,2,5]thiadiazolo[3,4-e]thieno[2'',3'':4',5']thieno[2',3':4,5]pyrrolo[3,2-g]thieno[2',3':4,5]thieno[3,2-b]indole-2,10-diyl)bis(methanylylidene))bis(5,6-difluoro-3-oxo2,3-dihydro-1H-indene-2,1-diylidene))dimalononitrile (L8-BO) acceptor, we designed and synthesized two oligothiophene-based small molecule donors (SMDs), named (5Z,5'Z)-5,5'-(((1,3,4-thiadiazole-2,5-diyl)bis(3,4',4''-trioctyl-[2,2':5',2''-terthiophene]-5'',5-diyl))bis(methaneylylidene))bis(3-ethyl-2-thioxothiazolidin-4-one) (TDZ-3TR) and (5Z,5'Z)-5,5'-(((1,3,4-selenadiazole-2,5-diyl)bis(3,4',4''-trioctyl-[2,2':5',2''-terthiophene]-5'',5-diyl))bis(methaneylylidene))bis(3-ethyl-2-thioxothiazolidin-4-one) (SeDZ-3RT), by bridging 1,3,4-thiadiazole (TDZ) or 1,3,4-selenadiazole (SDZ) and 3-ethylrhodanine terminals with terthiophene derivatives (Scheme 1). Replacing TDZ with SeDZ resulted in higher crystallinity of SeDZ-3TR and lowered its miscibility with L8-BO acceptor. Employing the resulting SMDs in the all-small molecule solar cells, poor performances were obtained due to the strong aggregation of these SMDs and sever phase separation of the SMD:L8-BO blend films. Adding a trace amount of SeDZ-3TR realized a better fibril network of L8-BO layer. On the other hand, two donor polymers of poly{[4,8-bis[5-(2-ethylhexyl)-4-fluoro-2-thienyl]benzo[1,2-b:4,5-b']-dithiophene-2,6-diyl]-alt-[2,5-thiophenediyl[5,7-bis(2ethylhexyl)-4,8-dioxo-4H,8H-benzo[1,2-c:4,5-c']dithiophene1,3-diyl]]} (PM6) and poly[(2,6-(4,8-bis(5-(2-ethylhexyl)-3-fluoro)thiophen-2-yl)benzo[1,2-b:4,5-b0]dithiophene))-alt-5,50-(5,8-bis(4-(2-butyloctyl)thiophen-2-yl)dithieno[3',2':3,4;2'',3'':5,6]benzo[1,2-

c][1,2,5]thiadiazole)] (D18) with different fibril widths and lengths were put together to optimize the fibril network of the donor layer. Finally, by depositing the fibrous L8-BO layer into the optimal PM6:D18 fibril mesh, a double-fibril network structure could be realized for improving the exciton diffusion and charge carrier transport. As a result, a high PCE of 19.38% was obtained in the relative LbL-OSCs, which is among the highest values for OSCs.



**Scheme 1.** a) The chemical structures of TDZ-3TR, SeDZ-3TR, PM6 and L8-BO. b) The synthetic routes of TDZ-3TR and SeDZ-3TR.

## Results and Discussion

### Materials Synthesis and Thermal Properties

The synthetic routes of the SMDs are shown in Scheme 1b. The cyclization reaction of compound 1 in the presence of Lawesson's reagent and Woollin's reagent afforded compounds 2a and 2b, respectively. Compounds 2a and 2b were lithiated and followed by quenching with trimethyltin chloride to obtain compounds 3a and 3b, respectively. Finally, TDZ-3TR and SeDZ-3TR were obtained through the Knoevenagel condensation of the compounds 5a and 5b with compound 6, respectively. The molecular structures were verified by nuclear magnetic resonance (NMR) spectra and mass spectra (see Supporting Information for details). Both SMDs show excellent solubility in common solvents, such as chlorobenzene (CB) and chloroform (CF). In addition, they also have good thermal stability with a high

decomposition temperature ( $T_d$ , 5% weight loss) of 366 °C (Figure S1). As determined by differential scanning calorimetry (DSC) measurements, SeDZ-3TR showed higher melting and crystallization points of 197.5 and 157.2 °C than those of 156.6 and 124.1 °C for TDZ-3TR, suggesting the higher crystallinity of former case (Figure 1a).

### Optical and Electrochemical Properties and Application as Electron Donors

The UV-vis absorption spectra of TDZ-3TR and SeDZ-3TR in diluted CF solutions and as films showed very similar profiles because they shared similar backbones (Figure 1b,c). Replacing TDZ with SeDZ resulted in slightly blue-shifted absorption of SeDZ-3TR than TDZ-3TR, possibly due to the lower electron deficient SeDZ weakened the intramolecular charge transfer (ICT) of SeDZ-3TR. From solution to film state, both molecules exhibited noteworthy redshifted absorption more than 100 nm (110 nm for TDZ-3TR and 112 nm for SeDZ-3TR), indicating their significantly enhanced molecular packing in film state. Compared to TDZ-3TR, SeDZ-3TR showed much stronger 0-0 absorption peak than 0-1 peak, suggesting the more ordered packing of SeDZ-3TR. This is in consistent with the higher crystallinity observed in DSC measurements. Their optical bandgaps ( $E_g^{\text{opt}}$ ) were estimated to be 1.81 eV for TDZ-3TR and 1.86 eV for SeDZ-3TR, respectively.

The frontier orbital levels of the two SMDs were measured by cyclic voltammetry (CV) experiments (Figure S2). The highest occupied molecular orbital (HOMO) and lowest unoccupied molecular orbital (LUMO) levels were determined to be  $-5.34$ ,  $-3.64$  eV and  $-5.38$ ,  $-3.67$  eV for TDZ-3TR and SeDZ-3TR, respectively, matching with the nonfullerene acceptors such as L8-BO (Figure 1d).

The application potential of TDZ-3TR and SeDZ-3TR as electron donors in OSCs was studied by fabricating OSCs with a conventional structure of ITO/PEDOT:PSS/SMD:L8-BO/PNDIT-F3N/Ag. Although DZ-3TR and SeDZ-3TR had good complementary absorption and matched energy levels with L8-BO, very low short current density ( $J_{sc}$ ) and fill factor (FF) were obtained in the OSCs, which led to their poor PCEs (Figure 1e). Specifically, TDZ-3TR:L8-BO-based devices achieved an open-circuit voltage ( $V_{oc}$ ) of 0.77 V, a  $J_{sc}$  of 2.66 mA cm<sup>-2</sup>, and an FF of 26.9%, limiting the PCE to 0.55% (Table S1).

Although higher  $V_{oc}$  of 0.82 V and FF of 29.7% were obtained, SeDZ-3TR:L8-BO-based devices obtained a lower PCE of 0.16%, due to the largely reduced  $J_{sc}$  of  $0.64 \text{ mA cm}^{-2}$ . The low current output was confirmed by the external quantum efficiency (EQE) measurements (Figure 1f).

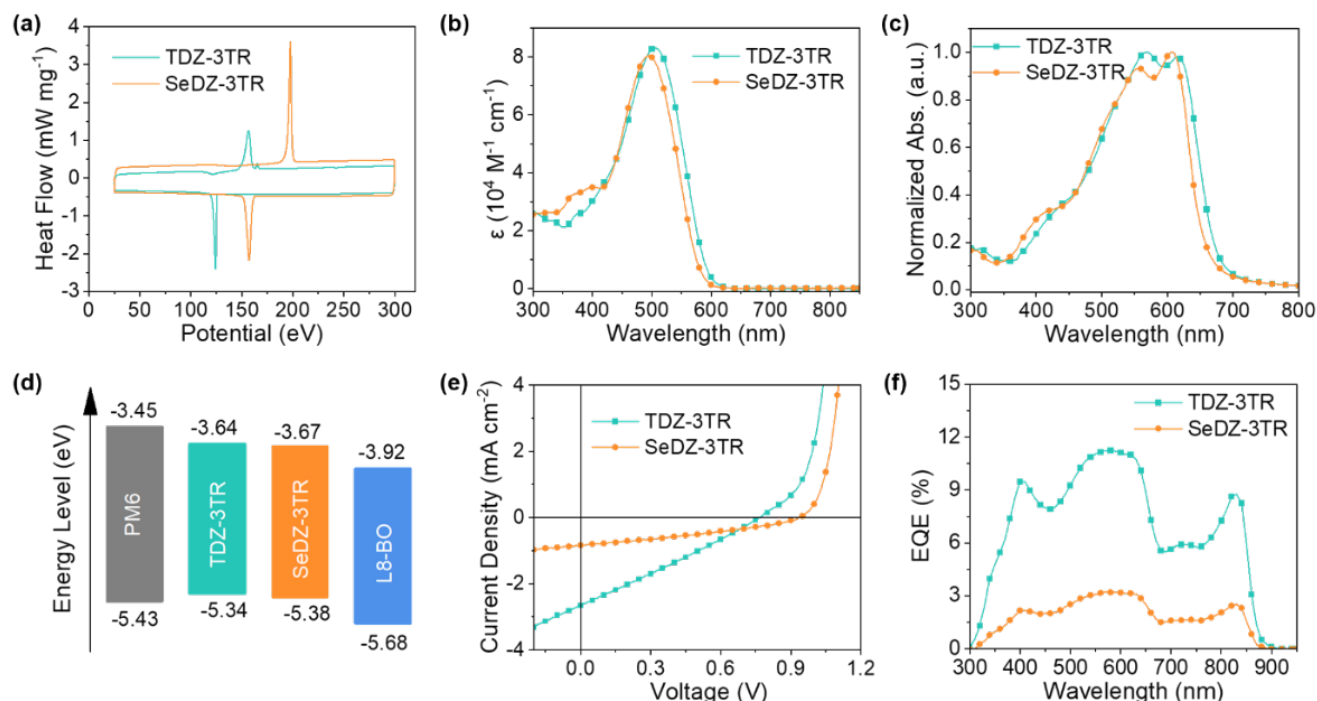


**Figure 1.** a) DSC curves of the SMDs. b) Molar extinction coefficient profiles of the SMDs in CF solution, c) Normalized UV-vis-IR absorption of the SMD films. d) Energy level diagram. e)  $J$ - $V$  curves of the OSCs based on SMD:L8-BO. f) EQE spectra of the OSCs based on SMD:L8-BO.

## Morphology Studies

To find the reason why these SMDs could not work well as electron donor in all-small molecule solar cells, the blend morphology was investigated by atomic force microscopy (AFM) measurements (Figure 2 and Figure S3). The relatively linear shape of TDZ-3TR and SeDZ-3TR made them had very strong aggregation tendency, resulting in poor film forming with many pinholes in their pristine films. The root-mean-square roughness ( $R_q$ ) was as large as 8.9 nm for TDZ-3TR and 10.9 nm SeDZ-3TR, respectively. In contrast the banana shape of L8-BO prevented it to form large crystals, resulting in a more smooth and uniform thin film with a small  $R_q$  of 0.45 nm. TDZ-3TR:L8-BO (1:1) blend exhibited quite inhomogeneous phase separation with a large  $R_q = 3.25 \text{ nm}$ . Compared with TDZ-3TR:L8-BO (1:1) blend, the SeDZ-3TR:L8-BO (1:1) blend exhibited more sever morphology, where large domains could be

observed and the  $R_q$  was increased to 4.78 nm. The stronger phase separation of SeDZ-3TR:L8-BO (1:1) blend with larger fibril width could be due to the higher crystallinity of SeDZ-3TR and its lower miscibility with L8-BO.

The crystallinity of the two SMDs were studied by Grazing incidence wide angle X-ray scattering (GIWAXS) experiments (Figure S4 and Table S2). Both TDZ-3TR and SeDZ-3TR exhibited well defined (100), (200), (300), and (400) diffractions in the out-of-plane direction and (010) diffraction in the in-plane direction, showing their preferred edge-on packing with high ordered crystallinity. SeDZ-3TR had a larger lamellar stacking distance ( $d_l$ ) of 2.17 nm ( $q_z = 2.89 \text{ nm}^{-1}$ ) than that of 2.14 nm ( $q_z = 2.94 \text{ nm}^{-1}$ ) for TDZ-3TR. However, SeDZ-3TR showed a smaller  $\pi$ - $\pi$  stacking distance ( $d_\pi$ ) of 0.361 nm ( $q_{xy} = 17.4 \text{ nm}^{-1}$ ) than that of 0.365 nm ( $q_{xy} = 17.2 \text{ nm}^{-1}$ ) for TDZ-3TR. Moreover, SeDZ-3TR showed higher crystal coherence lengths (CCLs) for both lamellar stacking (28.1 nm vs 26.4 nm) and  $\pi$ - $\pi$  stacking (10.5 nm vs 8.88 nm) than that of TDZ-3TR. These results demonstrated the higher crystallinity of SeDZ-3TR than TDZ-3TR.

The miscibility between these SMDs and L8-BO was predicted by droplet contact angle measurements (Figure S5). The surface energies ( $\gamma$ ) were determined to be 36.2 and 40.3  $\text{mJ m}^{-2}$  for PM6 and L8-BO, respectively. The  $\gamma$  of TDZ-3TR was 38.6  $\text{mJ m}^{-2}$ , which was almost in the middle of PM6 and L8-BO. In contrast, SeDZ-3TR had a lower  $\gamma$  of 36.7  $\text{mJ m}^{-2}$ , which was quite close to that of PM6 donor. The larger  $\gamma$  differences between SeDZ-3TR and L8-BO suggested the lower miscibility between them, resulting in stronger phase separation in the active blend. These might explain why SeDZ-3TR-based devices got lower  $J_{sc}$  and PCE than TDZ-3TR-based devices. To optimize the morphology, we tried to reduce the feeding ratio of these SMDs in the active blend. To our excited, with only 5wt% of these SMDs (relative to L8-BO) added to the L8-BO solution, fibril like morphology could be realized well in the corresponding thin films (Figure 2). In comparison, adding trace amount of these SMDs into the PM6 solution exerted minimal change on the morphology of the PM6 donor film (Figure S6). Therefore, introducing these SMDs into the acceptor layer might have more favorable impact on the performance of the LbL-OSCs than that into the donor layer.

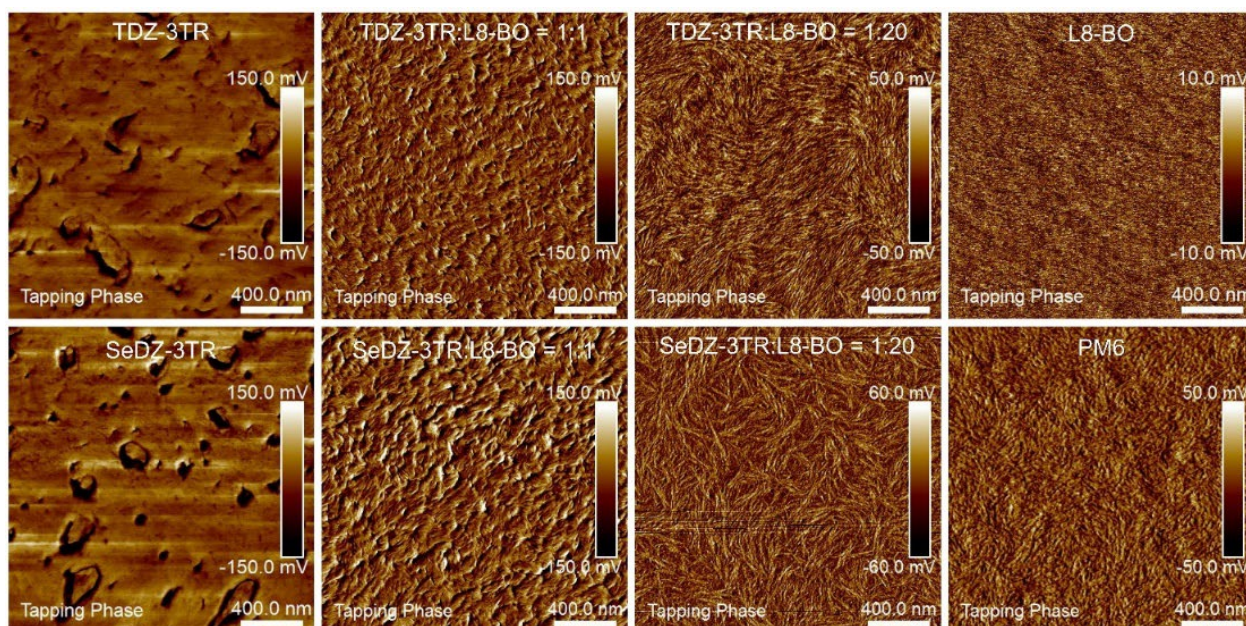


**Figure 2.** AFM phase images of the different thin films.

### Application as Additives in LbL-OSCs

The fibrous L8-BO layer observed in the AFM images encouraged us to introduce it into the PM6 fibril mesh to form a double-fibril network morphology for improving the exciton diffusion and charge carrier transport in the LbL-OSCs. The LbL-OSCs were fabricated and evaluated with a device structure of ITO/PEDOT:PSS/PM6/L8-BO (without or with SMDs)/PNDIT-F3N/Ag (Figure 3 and Table 1). The control devices without additive achieved a high  $V_{oc}$  of 0.905 V but a relatively low  $J_{sc}$  of  $24.50 \text{ mA cm}^{-2}$  and FF of 73.00%, limiting the PCE to 16.19%. By adding 2.5wt% of TDZ-3TR into the L8-BO layer, the  $J_{sc}$  and FF were increased to  $25.18 \text{ mA cm}^{-2}$  and 74.75%, respectively, thus improving the PCE to 16.95%. While adding 5.0wt% of TDZ-3TR further increased the  $J_{sc}$  and FF to  $25.62 \text{ mA cm}^{-2}$  and 77.35%, respectively, resulting in a higher PCE of 17.91%. While introducing TDZ-3TR more than 5wt% led to the simultaneously decreased  $V_{oc}$ ,  $J_{sc}$ , and FF, thus lowering the PCE in the corresponding LbL-OSCs. Similar variation trends could also be observed by replacing TDZ-3TR with SeDZ-3TR. With 2.5wt% of SeDZ-3TR introduced into the L8-BO layer, the  $J_{sc}$  and FF were increased to  $25.44 \text{ mA cm}^{-2}$  and 75.40%, respectively, thus enhancing the PCE to 17.42%. Adding 2.5wt% of SeDZ-3TR into the L8-BO layer, the higher  $J_{sc}$  of  $26.04 \text{ mA cm}^{-2}$  and FF of 78.55% contributed to a champion PCE of 18.59%. By adding

7.5wt% of SeDZ-3TR, the PCE was slightly reduced to 18.10%. Adding 10wt% of SeDZ-3TR, the PCE was further lowered to 17.41%. Compared to that incorporating these SMDs in the L8-BO acceptor layer, adding them into the PM6 layer exhibited minimal effect on the photovoltaic performances (Figure S7 and Table 3). These results indicated that TDZ-3TR and SeDZ-3TR could only be applied as additives in the acceptor layer to improve the device performance of LbL-OSCs. Moreover, the addition of these SMDs as the additives exhibited no negative influence on the device stability, over 90% of the origination PCE could be retained after 500 h continuous illumination (Figure S8).

The performance improvement was confirmed by the EQE measurements (Figure 2b,d). The increased EQE response after adding these SMDs in the L8-BO layer confirmed the improvement of the  $J_{sc}$  in the corresponding LbL-OSCs (Table 1). One of the reasons could be the improved absorbance by adding these SMDs. As shown in Figure S9, the absorption in the whole range was improved by adding 5wt% of these SMDs, which could contribute to the  $J_{sc}$  improvement of the corresponding devices. The enhanced absorption in shorter wavelength range (300–700 nm) was originated from the absorption of these SMDs. While the enhanced absorption longer wavelength range (700–950 nm) could be due to the enhanced molecular packing and fibrilization of L8-BO induced by these additives.

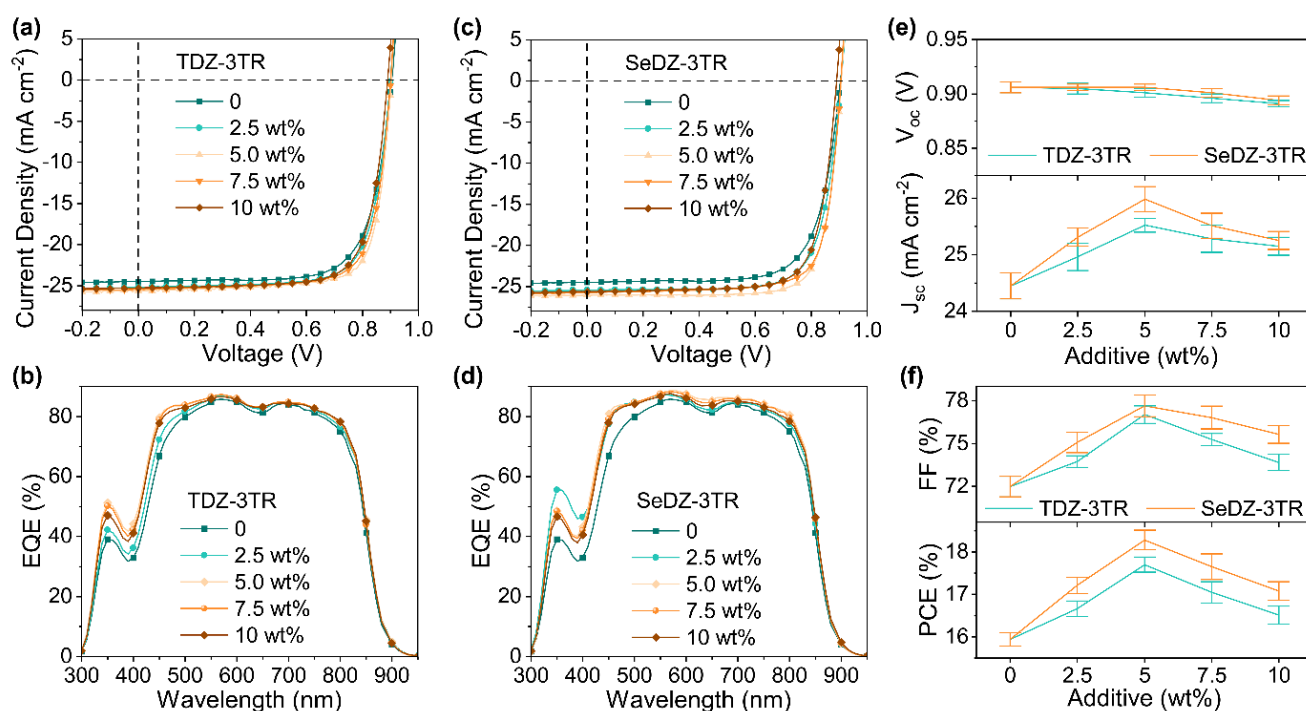


**Figure 3.** a)  $J$ - $V$  curves, and b) EQE curves of LbL-OSCs with different amounts of TDZ-3TR in the acceptor layer. c)  $J$ - $V$  curves, and d) EQE curves of LbL-OSCs with different amounts of SeDZ-3TR in the acceptor layer. e) The additive amount-dependent  $V_{oc}$  and  $J_{sc}$  for the LbL-OSCs. f) The additive amount-dependent FF and PCE for the LbL-OSCs.

**Table 1.** Photovoltaic parameters of the LbL-OSCs with various amounts of additives in the acceptor layer.

Additive	$V_{oc}$ [V]	$J_{sc}$ [mA cm <sup>-2</sup> ]	$J_{EQE}^{[b]}$ [mA cm <sup>-2</sup> ]	FF [%]	PCE [%]
w/o	0.905 (0.906±0.003) <sup>[a]</sup>	24.50 (24.45±0.23)	23.54	73.00 (71.98±0.72)	16.19 (15.94±0.16)
TDZ-3TR	0.900	25.18	24.18	74.75	16.95
2.5 wt%	(0.905±0.005)	(24.96±0.24)		(73.74±0.40)	(16.66±0.18)
TDZ-3TR	0.904	25.62	24.76	77.35	17.91
5 wt%	(0.901±0.004)	(25.52±0.12)		(77.02±0.61)	(17.70±0.18)
TDZ-3TR	0.896	25.45	24.66	75.63	17.32
7.5 wt%	(0.896±0.004)	(25.28±0.24)		(75.28±0.42)	(17.05±0.25)
TDZ-3TR	0.891	25.27	24.54	74.99	16.89
10 wt%	(0.891±0.003)	(25.15±0.16)		(73.67±0.57)	(16.51±0.21)
SeDZ-3TR	0.908	25.44	24.68	75.40	17.42
2.5 wt%	(0.906±0.003)	(25.31±0.16)		(75.08±0.71)	(17.21±0.19)
SeDZ-3TR	0.908	26.04	25.16	78.55	18.59
5 wt%	(0.906±0.004)	(25.98±0.22)		(77.64±0.76)	(18.28±0.23)
SeDZ-3TR	0.907	25.78	24.99	77.43	18.10
7.5 wt%	(0.901±0.004)	(25.51±0.22)		(76.81±0.79)	(17.65±0.30)
SeDZ-3TR	0.892	25.62	24.75	76.20	17.41
10 wt%	(0.894±0.004)	(25.25±0.16)		(75.63±0.62)	(17.08±0.22)

[a] The averaged values with standard deviations in the parentheses were calculated from 20 individual devices. [b] The integrated current densities were calculated from the EQE curves.

### Molecular Crystallinity and Charge Transport Properties

Grazing incidence wide angle X-ray scattering (GIWAXS) experiments were performed to study the effect of these SMDs on the crystallinity and molecular packing behaviors (Figure 4). The pristine L8-BO film showed a preferred face-on packing with a (11-1) peak around  $q_{xy} = 3.97 \text{ nm}^{-1}$  and (010) peak around  $q_z = 17.7 \text{ nm}^{-1}$ , corresponding to a  $d_{||}$  of 1.58 nm and a  $d_{\perp}$  of 0.355 nm (Table S2). Adding the two

SMDs had no impact on the packing orientation and distances; however, the crystal coherence lengths (CCLs) for the lamellar/ $\pi$ - $\pi$  stackings were increased from 5.78/2.42 nm for the pristine L8-BO film to 5.82, 2.63 nm for TDZ-3TR, and 5.86, 2.74 nm for SeDZ-3TR modified films, respectively, suggesting the slightly improved molecular crystallinity. The same phenomena could be observed in the sequentially deposited PM6/L8-BO film. The control PM6/L8-BO film exhibited a (100) peak at  $q_{xy} = 2.77 \text{ nm}^{-1}$  ( $d_l = 2.27 \text{ nm}$ , CCL = 10.1 nm) and a (11-1) peak at  $q_{xy} = 4.05 \text{ nm}^{-1}$  ( $d_\pi = 1.55 \text{ nm}$ , CCL = 9.48 nm), which could be assigned to the lamellar packing of the PM6 donor and L8-BO acceptor, respectively. In addition, a (010) peak at  $q_z = 17.5 \text{ nm}^{-1}$  was assigned to the sum of PM6 and L8-BO  $\pi$ - $\pi$  stackings which could not be divided. After adding these SMDs, the CCLs for the (100)/(11-1) peaks were increased to 11.2, 9.87 nm for TDZ-3TR, and 11.8, 10.3 nm for SeDZ-3TR modified PM6/L8-BO films, respectively. And the  $d_\pi$  was decreased from 0.359 nm for the control PM6/L8-BO film to 0.357 and 0.355 nm for TDZ-3TR and SeDZ-3TR modified PM6/L8-BO films, respectively, suggesting the improved crystallinity of the PM6/L8-BO film by adding these SMDs.

The improved molecular crystallinity could have positive effect on the charge transport. To study the effect on introducing these SMDs on the charge transport properties, space charge limited current experiments were conducted (Figure S10). the control PM6/L8-BO film without additive showed a hole mobility ( $\mu_h$ ) of  $4.1 \times 10^{-4} \text{ cm}^2 \text{ V}^{-1} \text{ s}^{-1}$  and an electron mobility ( $\mu_e$ ) of  $2.7 \times 10^{-4} \text{ cm}^2 \text{ V}^{-1} \text{ s}^{-1}$ . After adding additives, the  $\mu_h/\mu_e$  values were increased to  $6.5 \times 10^{-4}/4.9 \times 10^{-4} \text{ cm}^2 \text{ V}^{-1} \text{ s}^{-1}$  for TDZ-3TR, and  $7.3 \times 10^{-4}/6.2 \times 10^{-4} \text{ cm}^2 \text{ V}^{-1} \text{ s}^{-1}$  for SeDZ-3TR modified PM6/L8-BO films, respectively. As expected, the fibrilization of L8-BO and the increased crystallinity of the PM6/L8-BO film by adding these additives significantly improved the charge transport in the corresponding films.

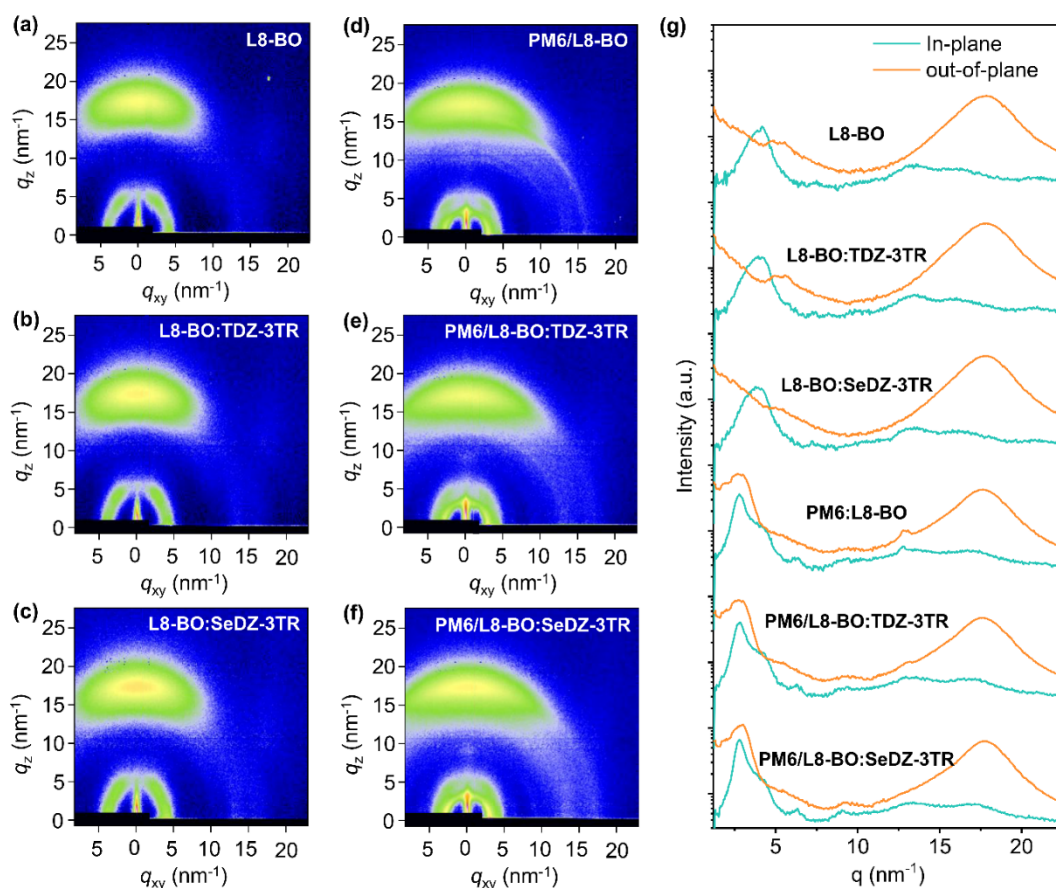


**Figure 4.** a-f) GIWAXS patterns of PM6 and PM6/L8-BO films without and with SMDs. g) The corresponding in-plane and out-of-plane line-cuts.

### Charge Generation and Recombination Kinetics

The charge generation kinetics affected by the SMDs was studied by femtosecond transient absorption spectroscopy (fs-TAS) measurements (Figure 5). An excitation wavelength of 780 nm was used to selectively excite L8-BO and study the hole transfer from acceptor to donor. The immediately absorption decay around 820 nm was assigned to the ground-state bleach (GSB) of L8-BO upon excitation, and the increased followed by decreased absorption around 630 nm was assigned to the GSB of PM6, suggesting the hole-transfer process from L8-BO to PM6. The rising kinetics of PM6 at 630 nm was fitted via a biexponential function, in which a fast component ( $\tau_1$ ) and slow component ( $\tau_2$ ) denoted the kinetics of the exciton dissociation at the D/A interfaces and exciton diffusion before reaching the D/A interfaces, respectively (Figure 5g). The control PM6/L8-BO film achieved a  $\tau_1$  of 0.44 ps and  $\tau_2$  of 17.9 ps, respectively. Introducing TDZ-3TR could lower  $\tau_1$  and  $\tau_2$  to 0.36 and 16.5 ps, respectively, indicating the

improved molecular interaction of donor and acceptor at the interfaces and enhanced exciton diffusion in the acceptor domains. Employing SeDZ-3TR as the additive,  $\tau_1$  and  $\tau_2$  were further reduced to 0.28 and 14.7 ps, respectively, indicating the more faster hole transfer in the corresponding photoactive layer. These could be attributed to the fibrilization of L8-BO afforded more efficient channels benefiting the hole transfer in the related PM6/L8-BO films.

To get insight of the effect of L8-BO fibrilization on the charge extraction process, transient photocurrent (TPC) measurements were performed (Figure 5h). By fitting the TPC decay kinetics, the charge extraction times of the LbL-OSCs were estimated to be 0.37, 0.34 and 0.31  $\mu\text{s}$  for the control devices, TDZ-3TR, and SeDZ-3TR modified devices, respectively. Moreover, the charge recombination information was studied by transient photovoltage (TPV) measurements (Figure 5i). By fitting the TPV decay kinetics, the charge lifetimes were estimated to be 9.2, 10.9 and 12.1  $\mu\text{s}$  for the control devices, TDZ-3TR, and SeDZ-3TR modified devices, respectively. The prolonged charge lifetimes and lowered charge extraction time by adding these SMDs could benefit the more efficient charge extraction and suppress the charge recombination, thus improving the device performances in the corresponding LbL-OSCs.

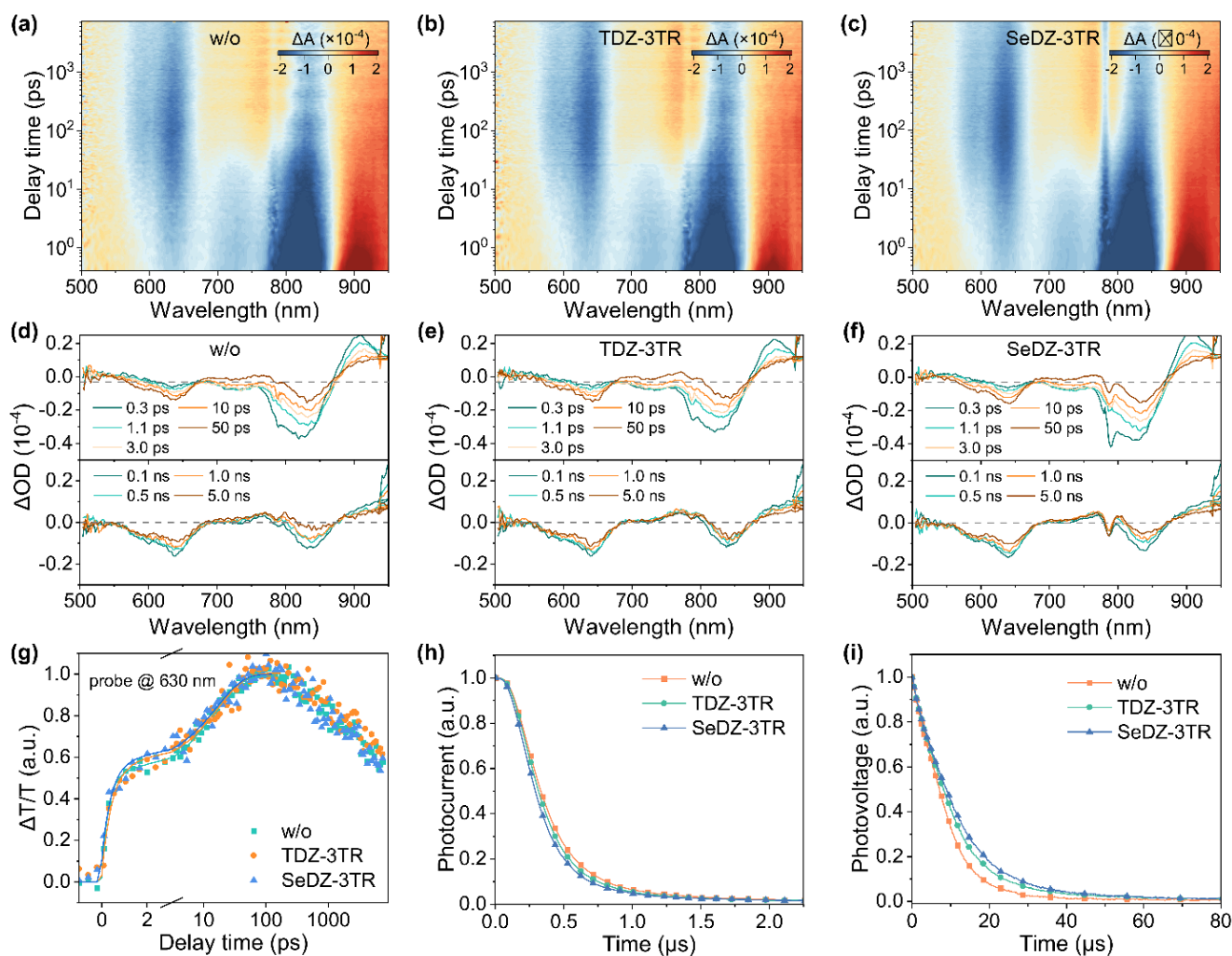


**Figure 5.** a-c) Color plots the fs-TA spectra of the PM6/L8-BO films without and with different additives. d-f) The corresponding TA spectra from (a-c). g) TA kinetics of the PM6/L8-BO films without and with different additives. h) TPC kinetics, and i) TPV kinetics of the LbL-OSCs without and with different additives.

### Donor Fibril Network Optimization for Improving the Performances

As observed in the AFM images (Figure 2), the as-cast PM6 layer deposited from the CF solution exhibited quite slender fibrils, which might also require further optimization to a more ideal fibril network. To increase the fibril width and length, another efficient polymer donor of D18 was introduced because it has stronger aggregation tendency and be more readily to form large fibrils. As shown in Figure S11, the prisitine D18 film showed noticeably larger fibrils than that of prisitine PM6 film. By adding D18 into PM6 solution, the resulng films exhibited stepwise modulated texture with gradually improved fibril width and length. Among them, donor layer with 25 wt% of D18 added exhibited more apporperiate

fibril network, which might benefit the hole transport in the related devices. As expected, replacing the pristine PM6 layer with such an optimized donor layer, the LbL-OSCs realized further improved PCE up to 19.38%, higher than the control PM6 (PCE = 18.59%) and D18 (PCE = 18.33%) based LbL-OSCs (Figure 6b,c and Table S4). Such a high PCE is among the best values for LbL-OSCs. The morphology of the optimized PM6:D18/L8-BO:SeDZ-3TR thin film (with 25 wt% of D18 in the donor layer and 5wt% SeDZ-3TR in the acceptor layer) was studied by AFM and photo-induced force microscopy (PiFM) measurements (Figure 6c-f). A well defined nanofibril network could be observed from the AFM images. Moreover, as shown the PiFM images, both PM6 donor and L8-BO acceptor formed suitable nanofibers, demonstrating an ideal double-fibril network morphology realized in the LbL-processed active layer. Such an ideal double-fibril network morphology was beneficial for improving the exciton diffusion and charge carrier transport, thus enabling the improved device performances.

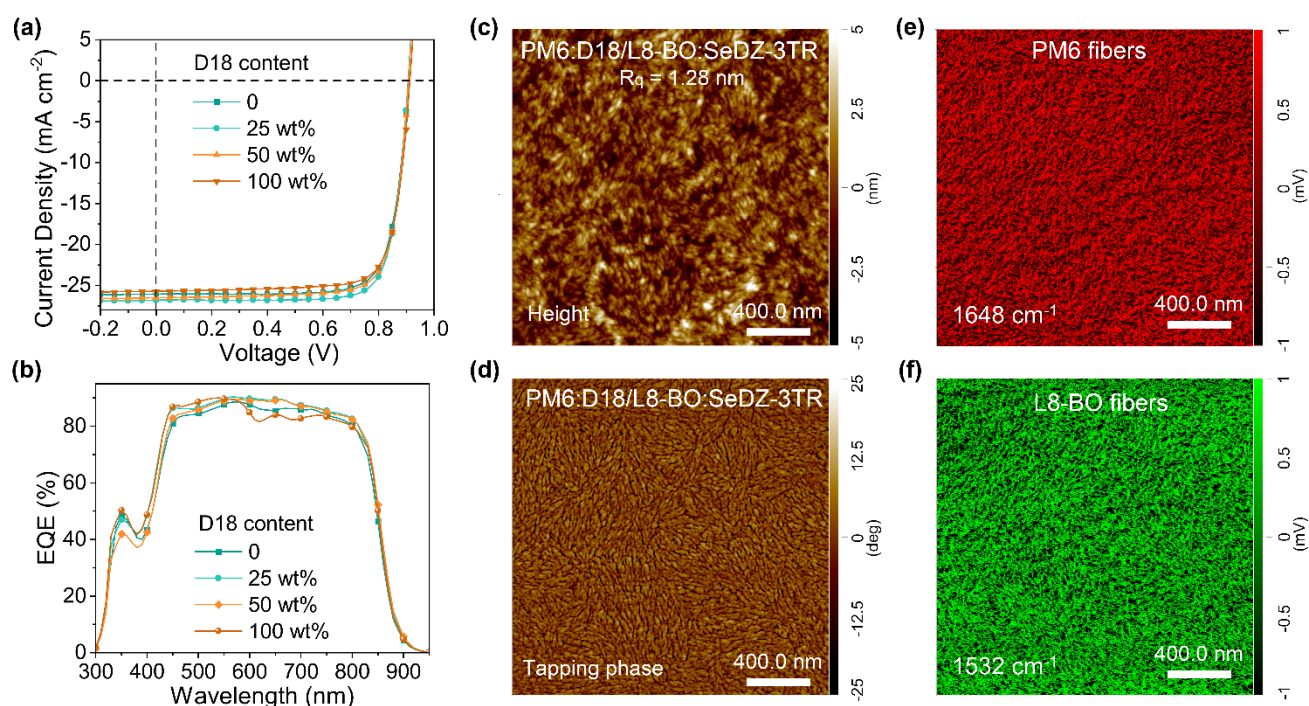


**Figure 6.** a) J-V curves, and b) EQE spectra of the LbL-OSCs based on PM6:D18/L8-BO:SeDZ-3TR with various ratios of D18 in the donor layer. c) AFM height image, d) AFM phase image, and e,f) PiFM images at a wave number of 1648  $\text{cm}^{-1}$  (representing PM6) 1532  $\text{cm}^{-1}$  (representing L8-BO) of the PM6:D18/L8-BO:SeDZ-3TR thin film (with 25 wt% of D18 in the donor layer and 5wt% SeDZ-3TR in the acceptor layer).

## Conclusion

In summary, we reported here the simultaneously fibril network optimization of acceptor and donor layers to construct an ideal double-fibril network morphology of the photoactive layer for high performance LbL-OSCs. To assist the fibrillization of L8-BO acceptor, we designed and developed two oligothiophene-based SMDs, named TDZ-3TR and SeDZ-3RT, by bridging 1,3,4-thiadiazole (TDZ) or 1,3,4-selenadiazole (SDZ) and 3-ethylrhodanine terminals with terthiophene derivatives. Replacing TDZ with SeDZ resulted in higher crystallinity of SeDZ-3TR and lowered its miscibility with L8-BO acceptor. Employing these SMDs in the all-small molecule solar cells, poor performances were obtained due to the strong aggregation of these SMDs and severe phase separation of the SMD:L8-BO blend films. However, adding trace amount of SeDZ-3TR realized a better fibril network of L8-BO layer. On the other hand, two donor polymers, PM6 and D18 with different fibril widths and lengths, were put together to optimize the fibril network of the donor layer. Finally, by depositing the fibrous L8-BO layer into the optimal PM6:D18 fibril mesh, a double-fibril network structure could be realized for improving the exciton diffusion and charge carrier transport. As a result, a high PCE of 19.38% was realized in the relative LbL-OSCs, much higher than the control LbL-OSCs based on as-cast PM6/L8-BO photoactive layer (16.19%). The results demonstrate the rational fibrillization of both the polymer and the acceptor layers is of great importance to realize an ideal double-fibril network for maximizing the device performances of LbL-OSCs.

## Supporting Information

Supporting Information is available from the Wiley Online Library or from the author.

## Acknowledgements

This work was financially supported by the National Key Research and Development Program of China (Grant No. 2022YFB4200500), National Natural Science Foundation of China (NSFC, 21825502, 22075190, 22105135 and 22379101), Sichuan Natural Science Foundation (2023NSFSC0304), Special Fund for Strategic Cooperation Between Sichuan University and Suining City (2022CDSN-01), and Special Fund for Strategic Cooperation Between Sichuan University and Dazhou City (2022CDDZ-04).

The authors also thank National Synchrotron Light Source II (NSLS-II, Contract No. DE-SC0012704) Brookhaven National Laboratory for providing GIWAXS experiment time.

Received: ((will be filled in by the editorial staff))

Revised: ((will be filled in by the editorial staff))

Published online: ((will be filled in by the editorial staff))

## References

- [1] X. Yang, Y. Shao, S. Wang, M. Chen, B. Xiao, R. Sun, J. Min, *Adv. Mater.* **2024**, *36*, 2307863.
- [2] C. Liu, L. Shao, S. Chen, Z. Hu, H. Cai, F. Huang, *Prog. Polym. Sci.* **2023**, *143*, 101711.
- [3] J. Yi, G. Zhang, H. Yu, H. Yan, *Nat. Rev. Mater.* **2024**, *9*, 46.
- [4] H. Yao, J. Wang, Y. Xu, S. Zhang, J. Hou, *Acc. Chem. Res.* **2020**, *53*, 822.
- [5] K. Liu, Y. Jiang, G. Ran, F. Liu, W. Zhang, X. Zhu, *Joule* **2024**, 10.1016/j.joule.2024.01.005.
- [6] M. Deng, X. Xu, Y. Duan, W. Qiu, L. Yu, R. Li, Q. Peng, *Adv. Mater.* **2024**, *36*, 2308216.
- [7] Z. Zhong, S. Chen, J. Zhao, J. Xie, K. Zhang, T. Jia, C. Zhu, J. Jing, Y. Liang, L. Hong, S. Zhu, D. Ma, F. Huang, *Adv. Energy Mater.* **2023**, *13*, 2302273.
- [8] J. Wang, Y. Wang, P. Bi, Z. Chen, J. Qiao, J. Li, W. Wang, Z. Zheng, S. Zhang, X. Hao, J. Hou, *Adv. Mater.* **2023**, *35*, 2301583.
- [9] B. Pang, C. Liao, X. Xu, S. Peng, J. Xia, Y. Guo, Y. Xie, Y. Chen, C. Duan, H. Wu, R. Li, Q. Peng, *Adv. Mater.* **2023**, *35*, 2211871.
- [10] D. Li, N. Deng, Y. Fu, C. Guo, B. Zhou, L. Wang, J. Zhou, D. Liu, W. Li, K. Wang, Y. Sun, T. Wang, *Adv. Mater.* **2023**, *35*, 2208211.
- [11] C. Guo, Y. Fu, D. Li, L. Wang, B. Zhou, C. Chen, J. Zhou, Y. Sun, Z. Gan, D. Liu, W. Li, T. Wang, *Adv. Mater.* **2023**, *35*, 2304921.
- [12] Q. Fan, R. Ma, Z. Bi, X. Liao, B. Wu, S. Zhang, W. Su, J. Fang, C. Zhao, C. Yan, K. Chen, Y. Li, C. Gao, G. Li, W. Ma, *Adv. Funct. Mater.* **2023**, *33*, 2211385.
- [13] T. Chen, S. Li, Y. Li, Z. Chen, H. Wu, Y. Lin, Y. Gao, M. Wang, G. Ding, J. Min, Z. Ma, H. Zhu, L. Zuo, H. Chen, *Adv. Mater.* **2023**, *35*, 2300400.
- [14] L. Zhu, M. Zhang, J. Xu, C. Li, J. Yan, G. Zhou, W. Zhong, T. Hao, J. Song, X. Xue, Z. Zhou, R. Zeng, H. Zhu, C. C. Chen, R. C. I. MacKenzie, Y. Zou, J. Nelson, Y. Zhang, Y. Sun, F. Liu, *Nat. Mater.* **2022**, *21*, 656.
- [15] R. Yu, R. Shi, Z. He, T. Zhang, S. Li, Q. Lv, S. Sha, C. Yang, J. Hou, Z. Tan, *Angew. Chem. Int. Ed.* **2023**, *62*, e202308367.

- [16] M. Zhou, C. Liao, Y. Duan, X. Xu, L. Yu, R. Li, Q. Peng, *Adv. Mater.* **2023**, *35*, 2208279.
- [17] Y. Zhang, B. Wu, Y. He, W. Deng, J. Li, J. Li, N. Qiao, Y. Xing, X. Yuan, N. Li, C. J. Brabec, H. Wu, G. Lu, C. Duan, F. Huang, Y. Cao, *Nano Energy* **2022**, *93*, 106858.
- [18] X. Xu, L. Yu, H. Meng, L. Dai, H. Yan, R. Li, Q. Peng, *Adv. Funct. Mater.* **2022**, *32*, 2108797.
- [19] Z. Q. Liang, M. M. Li, Q. Wang, Y. P. Qin, S. J. Stuard, Z. X. Peng, Y. F. Deng, H. Ade, L. Ye, Y. H. Geng, *Joule* **2020**, *4*, 1278.
- [20] S. Liu, D. Chen, X. Hu, Z. Xing, J. Wan, L. Zhang, L. Tan, W. Zhou, Y. Chen, *Adv. Funct. Mater.* **2020**, *30*, 2003223.
- [21] R. Sun, J. Guo, Q. Wu, Z. Zhang, W. Yang, J. Guo, M. Shi, Y. Zhang, S. Kahmann, L. Ye, X. Jiao, M. A. Loi, Q. Shen, H. Ade, W. Tang, C. J. Brabec, J. Min, *Energy Environ. Sci.* **2019**, *12*, 3118.
- [22] Y. Zhang, G. Li, *Accounts Mater. Res.* **2020**, *1*, 158.
- [23] M. Li, Q. Wang, J. Liu, Y. Geng, L. Ye, *Mater. Chem. Front.* **2021**, *5*, 4851.
- [24] H. Fu, Z. Peng, Q. Fan, F. R. Lin, F. Qi, Y. Ran, Z. Wu, B. Fan, K. Jiang, H. Y. Woo, G. Lu, H. Ade, A. K. Y. Jen, *Adv. Mater.* **2022**, *34*, 2202608.
- [25] W. Gao, F. Qi, Z. Peng, F. R. Lin, K. Jiang, C. Zhong, W. Kaminsky, Z. Guan, C. S. Lee, T. J. Marks, H. Ade, A. K. Jen, *Adv. Mater.* **2022**, *34*, 2202089.
- [26] D. Zhang, W. Zhong, L. Ying, B. Fan, M. Li, Z. Gan, Z. Zeng, D. Chen, N. Li, F. Huang, Y. Cao, *Nano Energy* **2021**, *85*, 105957.
- [27] M. D. M. Faure, B. H. Lessard, *J. Mater. Chem. C* **2021**, *9*, 14.
- [28] R. Yu, X. Wei, G. Wu, Z. Tan, *Aggregate* **2021**, *3*, e107.
- [29] Q. He, W. Sheng, M. Zhang, G. Xu, P. Zhu, H. Zhang, Z. Yao, F. Gao, F. Liu, X. Liao, Y. Chen, *Adv. Energy Mater.* **2021**, *11*, 2003390.
- [30] X. Li, R. Zhu, Z. He, X. Du, H. Lin, C. Zheng, G. Yang, Z. Chen, S. Tao, *ACS Appl. Mater. Interfaces* **2022**, *14*, 25842.
- [31] X. Wang, L. Zhang, L. Hu, Z. Xie, H. Mao, L. Tan, Y. Zhang, Y. Chen, *Adv. Funct. Mater.* **2021**, *31*, 2102291.
- [32] R. Yu, G. Wu, Y. Cui, X. Wei, L. Hong, T. Zhang, C. Zou, S. Hu, J. Hou, Z. Tan, *Small* **2021**, *17*, 2103497.
- [33] C. He, Y. Pan, G. Lu, B. Wu, X. Xia, C. Q. Ma, Z. Chen, H. Zhu, X. Lu, W. Ma, L. Zuo, H. Chen, *Adv. Mater.* **2022**, *34*, 2203379.
- [34] S. Lai, Y. Cui, Z. Chen, X. Xia, P. Zhu, S. Shan, L. Hu, X. Lu, H. Zhu, X. Liao, Y. Chen, *Adv. Mater.* **2024**, *36*, 2313105.
- [35] X. Li, L. Cao, X. Yu, X. Du, H. Lin, G. Yang, Z. Chen, C. Zheng, S. Tao, *Solar RRL* **2022**, *6*.
- [36] S. Y. Park, C. Labanti, J. Luke, Y. C. Chin, J. S. Kim, *Adv. Energy Mater.* **2021**, *12*, 2103237.

- [37] C. Zhang, Z. Ge, J. Xue, W. Ma, Y. Sun, *Macromol. Chem. Phys.* **2022**, 224.
- [38] Y. Zhang, K. Liu, J. Huang, X. Xia, J. Cao, G. Zhao, P. W. K. Fong, Y. Zhu, F. Yan, Y. Yang, X. Lu, G. Li, *Nat. Commun.* **2021**, 12, 4815.
- [39] K. Weng, L. Ye, L. Zhu, J. Xu, J. Zhou, X. Feng, G. Lu, S. Tan, F. Liu, Y. Sun, *Nat. Commun.* **2020**, 11, 2855.
- [40] L. Zhan, S. Li, X. Xia, Y. Li, X. Lu, L. Zuo, M. Shi, H. Chen, *Adv. Mater.* **2021**, 33, 2007231.
- [41] J. Wan, L. Zeng, X. Liao, Z. Chen, S. Liu, P. Zhu, H. Zhu, Y. Chen, *Adv. Funct. Mater.* **2021**, 32, 2107567.
- [42] S. Karuthedath, Y. Firdaus, A. D. Scaccabarozzi, M. I. Nugraha, S. Alam, T. D. Anthopoulos, F. Laquai, *Small Struct.* **2022**, 3, 2100199.
- [43] W. Xu, X. Ma, J. H. Son, S. Y. Jeong, L. Niu, C. Xu, S. Zhang, Z. Zhou, J. Gao, H. Y. Woo, J. Zhang, J. Wang, F. Zhang, *Small* **2022**, 18, 2104215.
- [44] H. Fu, W. Gao, Y. Li, F. Lin, X. Wu, J. H. Son, J. Luo, H. Y. Woo, Z. Zhu, A. K. Y. Jen, *Small Methods* **2020**, 4, 2000687.
- [45] J. Chen, J. Cao, L. Liu, L. Xie, H. Zhou, J. Zhang, K. Zhang, M. Xiao, F. Huang, *Adv. Funct. Mater.* **2022**, 32, 2200629.
- [46] K. Jiang, J. Zhang, Z. Peng, F. Lin, S. Wu, Z. Li, Y. Chen, H. Yan, H. Ade, Z. Zhu, A. K. Jen, *Nat. Commun.* **2021**, 12, 468.
- [47] J. Zhou, D. Li, L. Wang, X. Zhang, N. Deng, C. Guo, C. Chen, Z. Gan, C. Liu, W. Sun, D. Liu, W. Li, Z. Li, K. Wang, T. Wang, *Interdisciplinary Materials* **2023**, 2, 866.
- [48] L. Wang, C. Chen, Y. W. Fu, C. H. Guo, D. H. Li, J. C. Cheng, W. Sun, Z. R. Gan, Y. D. Sun, B. J. Zhou, C. H. Liu, D. Liu, W. Li, T. Wang, *Nat. Energy* **2024**, 9, 208.

The fibrilization of the small molecule acceptor by adding a trace amount of small molecule donors and fibril network optimization of the donor layer by introducing another polymer donor resulted in an optimal double-fibril network of the photoactive layer and an impressive power conversion efficiency of 19.38% for layer-by-layer organic solar cells.

X. Chen, Y. Li, W. Jing, T. Zhou, X. Xu,\* Y. Duan, L. Yu, R. Li, and Q. Peng\*

## Layer-by-Layer Organic Solar Cells Enabled by 1,2,4-Selenadiazole-Containing Crystalline Small Molecule with Double-Fibril Network Morphology

ToC figure (55 mm broad × 50 mm high)

